Nucleic Acids Research, 2005, Vol. 33, No. 7 ***e68***
doi:10.1093/nar/gni073

Analysis of scanning force microscopy images of protein-induced DNA bending using simulations

Remus T. Dame*, Joost van Mameren, Martijn S. Luijsterburg, Monika E. Mysiak[1], Ana Janićijević[2], Grzegorz Pazdzior, Peter C. van der Vliet[1], Claire Wyman[2,3] and Gijs J.L. Wuite

Physics of Complex Systems, Department of Physics and Astronomy, Faculty of Sciences, Vrije Universiteit, De Boelelaan 1081, NL-1081 HV, Amsterdam, The Netherlands, [1]Department of Physiological Chemistry, University Medical Center Utrecht and Centre for Biomedical Genetics, Utrecht, The Netherlands, [2]Department of Cell Biology and Genetics and [3]Department of Radiation Oncology, Erasmus MC, PO Box 1738, 3000 DR, Rotterdam, The Netherlands

Received December 23, 2004; Revised March 8, 2005; Accepted April 4, 2005

ABSTRACT

Bending of DNA is a feature essential to the function of many DNA-binding proteins. Bending angles can be estimated with a variety of techniques, but most directly from images obtained using scanning force microscopy (SFM). Direct measurement of the bending angle using a tangent method often produces angles that deviate significantly from values obtained using other techniques. Here, we describe the application of SFM in combination with simulations of DNA as a means to estimate protein-induced bending angles in a reliable and unbiased fashion. In this manner, we were able to obtain accurate estimates for the bending angles induced by nuclear factor I, octamer-binding transcription factor 1, the human XPC-Rad23B complex.

INTRODUCTION

DNA bending proteins play important roles in a wide range of biological processes. Locally, bending of DNA is used to promote functional contacts between proteins or between protein and DNA, e.g. in the regulation of transcription or DNA replication (1,2). At the level of global organization of bacterial chromosomal DNA, bending is important as a means of DNA compaction (3–5).

Various techniques are available for the measurement of protein-induced DNA bending angles. Estimates can be obtained from gel retardation experiments (6), DNA circularization experiments (7), co-crystal structures (8–10) and Förster resonance energy transfer (11–14). A limitation of these techniques is that the value obtained is usually an ensemble average and that possible sub-populations cannot be observed. Using scanning force microscopy (SFM), DNA bending can be directly evaluated in single complexes (15,16). The shape of the distribution provides insight into the nature of the bend. For example, different well-defined conformations would be reflected in a multi-modal distribution and flexibility of the bend would be reflected in the width of the distribution. Usually, these measurements are carried out by placing tangent vectors from the site of the bend after visual inspection. The outcome of the tangent method is not well defined, since the apparent bend depends on the image resolution, which in turn has an upper bound set by tip convolution effects (17). The outcome is also operator dependent (17), primarily since the approach taken in drawing tangents is not uniquely defined. As a consequence, bending angles thus estimated tend to deviate from values obtained using other techniques (18–20).

A method to avoid this has been proposed by Rivetti and co-workers. Their method, based on the worm-like chain model for semi-flexible polymers (21,22), describes the effect of local bends on the end-to-end distance (EED) of the polymer (17). They derived an expression for the bend angle as a function of contour length, persistence length and the mean-squared EED. This has been applied to DNA containing regions of high curvature or intrinsic flexibility (17,23) and to the analysis of protein-induced DNA bending (24). Using only the mean-squared EED value of a population of molecules, one might disregard information contained in the characteristic shape of the EED distribution. One of the disadvantages of this is that deposition anomalies may be concealed. We introduce an alternative method inspired by

*To whom correspondence should be addressed. Tel: +31 20 59 87 838; Fax: +31 20 59 87 991; Email: rtdame@nat.vu.nl

The authors wish it to be known that, in their opinion, the first two authors should be regarded as joint First Authors

the work of Rivetti *et al.* (17,24), yet employing the shape of the EED distribution instead of an average value, in order to obtain bend angles from SFM images in a controlled and well-defined manner. Since analytical expressions for these distributions exist exclusively for unbent polymers (25), we use simulations of large numbers of DNA molecules with varying bending parameters, to obtain EED distributions that indeed display a characteristic asymmetry. We employ these simulated distributions to fit experimentally obtained EED histograms for the DNA-bending proteins nuclear factor I (NFI), octamer-binding transcription factor 1 (Oct-1), the human XPC-Rad23B complex (XPC-HR23B) and integration host factor (IHF), thereby taking into account the distributions of EED values acquired from SFM images. Using this procedure, we estimate in a reliable and unbiased fashion bending angles induced by these proteins. This new method enables one to extend the analysis of DNA bending to cases in which one is forced to use mixed populations of bent/unbent DNA. Furthermore, bending configurations that are inaccessible to analytical approaches, such as flexible bends or multiple bends per DNA molecule, can be easily addressed.

MATERIALS AND METHODS

Sample preparation

A linear DNA fragment containing the IHF-site exactly at its centre was obtained by PCR from the vector pGP160 (26) using primer I (5′-GGCGTTATCCCATTTGCTCCAC-AGTGCCTCACGATCATAATCATGG-3′) and primer II (5′-CGTCCAGCTCACTACCCGGGCGTTTTTCTTCAGGT-AATGC-3′). Primer II was biotinylated at the 5′ end such that the resulting PCR product has a biotin at one of its ends. This primer was also designed such as to give rise to a unique SmaI site in the PCR product, which after digestion gives rise to a DNA molecule of 1075 bp. The biotinylated DNA (1–4 pmol) was immobilized on streptavidin-coated paramagnetic beads. After washing the DNA on the beads as described previously (27), the beads were resuspended in 10 µl BI (50 mM HEPES, pH 7.6, 60 mM KCl, 15 mM NaCl and10 mM $MgCl_2$). An aliquot of 2 pmol of IHF was added and the reaction mixture was incubated at 37° for 30 min. After removal of the liquid (to take away excess IHF), the beads were resuspended in 5 µl BI containing 2U of SmaI (New England Biolabs, Beverly, MA) and incubated for 1 h. An aliquot of 2 µl of the solution containing the IHF–DNA complexes was subsequently diluted 20 times into DB (2.5 mM HEPES, pH 7.6, 1.25 mM KCl and 5 mM $MgCl_2$). An aliquot of 12 µl of this mixture was subsequently deposited onto mica. After 1 min, the mica disc was gently rinsed with HPLC water and blown dry with argon.

NFI-, Oct-1- and XPC-HR23B–DNA complexes were prepared as described previously (28–30). The lengths of the respective DNA molecules were 711 bp (NFI and Oct-1) and 769 bp (XPC-HR23B).

Scanning force microscopy

Images of IHF–DNA complexes were acquired on a Nanotec microscope operating in tapping mode in air, with NanoDevices Metrology Probes. Images of NFI-, Oct-1 and XPC-HR23B–DNA complexes were acquired on a Nanoscope IIIa (Digital Instruments, Santa Barbara, CA) operating in tapping mode in air with silicon nanotips™ (Nanoprobe). The size of the DNA fragments used was in the range optimal for detecting changes in EED (roughly from 200 to 500 nm or from 600 to 1500 bp), as derived from the dependence of the mean-squared EED on an induced bend (17).

SFM image analysis

DNA molecules were selected for analysis after visual inspection of absence of overlaps with itself or others, as well as for the presence of bound protein (if its size permits). To measure the contour length and EED, DNA molecules were manually traced using Image SXM v. 1.69 (Steve Barrett, Surface Science Research Centre, University of Liverpool, UK). End points were chosen as being at the centre of the semicircle at the ends of the DNA molecule. Contour length and EED values used for further quantitative analysis were the average of 10 independent measurements.

The thus measured contour lengths of the respective DNA fragments were 352 nm (IHF), 233 nm (NFI and Oct-1) and 259 nm (XPC-HR23B), which results in a rise per base pair of 0.33 nm, well in agreement with that of B-form DNA (31). By comparing the contour lengths of bare and complexed DNA, we assured that the contour length of the DNA is not significantly affected by binding of the protein.

EED values were normalized by dividing the measured EED by the measured contour length of each individual molecule/complex. In the case of IHF–DNA complexes, bending angles were also estimated using the tangent method halfway each molecule's contour.

Fitting procedure

The end-to-end distributions obtained from our experiments were fitted using least-squares minimization to simulated histograms as follows. We first fitted the EED/*L* data from images of bare DNA controls to the simulated histograms for zero bending angle, to obtain the appropriate persistence lengths for these DNA templates and to ensure that they correspond with literature values. We then fitted the data from DNA bound by IHF, NFI, Oct-1 and XPC-HR23B to the simulated histograms corresponding to that persistence length, yielding a fit value for the induced bending angle.

In order to perform least-squares minimization in a statistically sound way, we used an expression for χ^2 (the mean-squared error) that is applicable to processes that are governed by Poisson statistics (32). To obtain the statistical uncertainty in the best-fit bending angle, we locate the intersections of the χ^2 profile with the minimum χ^2 value increased by 1 (33).

RESULTS AND DISCUSSION

Visualization of protein–DNA complexes

Our analysis of protein-induced DNA bending comprised the structural effects of the binding of four different proteins, IHF, Oct-1, NFI and XPC-HR23B, to their respective specific sites. The size of the DNA fragments used was in the range optimal for detecting changes in EED [roughly from 600 to 1500 bp (17)]. For the estimation of the NFI and Oct-1 induced bend, we analyzed the EED of NFI–DNA and Oct-1–DNA

complexes formed at the Ad5 wild-type origin and two mutant Ad5 origins by SFM. The bending by these proteins has been previously analyzed from SFM images using the tangent method (19,28–30) and/or with biochemical techniques (6,7,34). In this case, the relatively large size of NFI and Oct-1 allows the complexes to be easily distinguished from bare DNA molecules and, therefore, the data for the bare DNA and the complexes can be plotted as separate histograms. In a similar manner, we determined the EED of complexes between XPC-HR23B and a DNA fragment containing a defined damage at a known position (28). Finally, we tested our approach on IHF–DNA complexes for which (due to the small size of IHF) it is often not clear by simple visual inspection that protein is bound. In order to estimate the IHF-induced bend in DNA, we imaged IHF–DNA complexes by SFM (Figure 1a) and determined the EED of a mixed population of bare DNA and IHF–DNA complexes. In this case, all data were simultaneously plotted in a histogram, displaying a higher abundance of molecules with low EED than in control experiments with bare DNA (Figure 1b, top and bottom, respectively). The shoulder at low EEDs must therefore be attributed to IHF–DNA complexes.

Simulations

In order to predict the EED distributions for DNA molecules equilibrated in 2D space [as opposed to being projected from their 3D conformation (35)], we simulated DNA molecules as worm-like chains and constructed histograms of EED values. DNA molecules were simulated as a collection of segments, using custom-built LabVIEW™ software (National Instruments). The planar angles between consecutive segments (see Figure 2a) were drawn from a Gaussian distribution (36), the width of which is directly proportional to the persistence length P:

$$\langle(\Delta\theta)^2\rangle = \frac{kT\Delta s}{\kappa} = \frac{\Delta s}{P}, \quad \mathbf{1}$$

where Δs is the length of a segment, κ is the bending modulus and kT is the available thermal energy. The Gaussian shape of the angle distribution ensures the chain to be worm-like, whereas a uniform distribution would yield freely jointed chains. This was independently confirmed by the calculation of the persistence length for thus obtained chains from its defining equation,

$$\langle\cos(\Delta\theta(s))\rangle = \exp(-s/2P), \quad \mathbf{2}$$

which indeed reproduced the persistence length that was imposed in the simulation. In all simulations, the molecules consisted of 1000 segments, rendering a single segment to be shorter than a base pair. Increasing the number of segments did not influence the simulations.

An additional, fixed bend was introduced at a given segment, generating a polymer chain similar to that shown in Figure 2b. For each simulated molecule, the value of

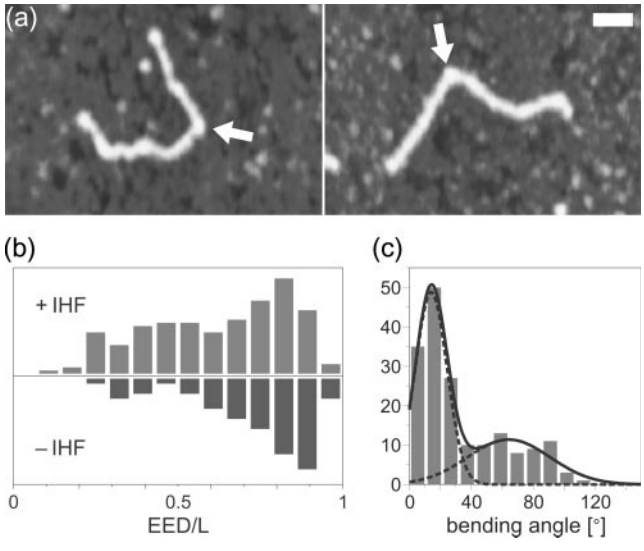

Figure 1. (**a**) Typical IHF–DNA complexes imaged as described in Materials and Methods. The protein-induced bend is indicated by the arrows. Owing to its size, the IHF protein cannot be unambiguously identified in the images, demonstrating the need for an analytical approach using other than visual characteristics. The scale bar is 50 nm. Gray scale represents height ranging from 0 nm (dark) to 2 nm (bright). (**b**) Distributions of EED values normalized by contour lengths L of IHF–DNA complexes (top) and bare DNA molecules (bottom), demonstrating the effect of DNA bending. (**c**) Histogram of bending angles estimated using tangents from IHF–DNA complexes. The bimodal distribution shows that not all DNA molecules have IHF bound; by fitting to a double Gaussian distribution, we estimate that ~50% of the imaged molecules have IHF bound.

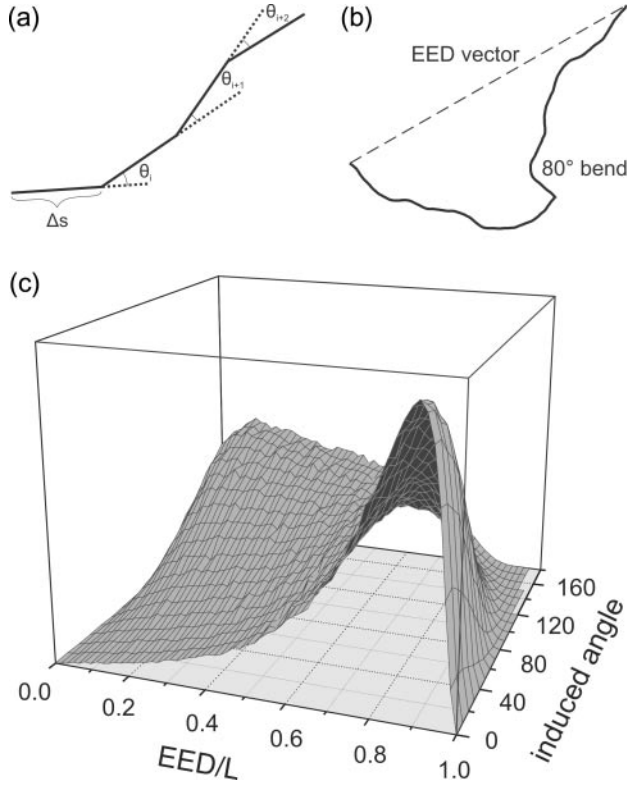

Figure 2. Simulation of DNA molecules equilibrated on a surface. (**a**) Definition of the polymer quantities in Equation 1. (**b**) Simulated molecule with a contour length $L = 4P$ and an 80° bend at 50% of its contour length; the dashed line indicates the end-to-end vector. (**c**) Normalized EED histograms for such molecules with angles ranging from 0° to 160°. Each histogram is based on 100 000 simulated molecules.

the EED is stored as a fraction of its contour length, *L*. We generated histograms of EED/*L* values of 100 000 simulated molecules for many combinations of parameters (persistence length, bending angle and bending location along DNA). Results for $L = 4P$ polymers with induced angles ranging from 0° to 160° are shown in Figure 2c. Since the equilibration of linear DNA on a surface almost always leads to non-overlapping molecules, we included self-avoidance in our simulations by simply rejecting self-crossing chains from the histograms. We found only very small deviations exclusively at high bending angles, rendering this computationally expensive procedure unnecessary.

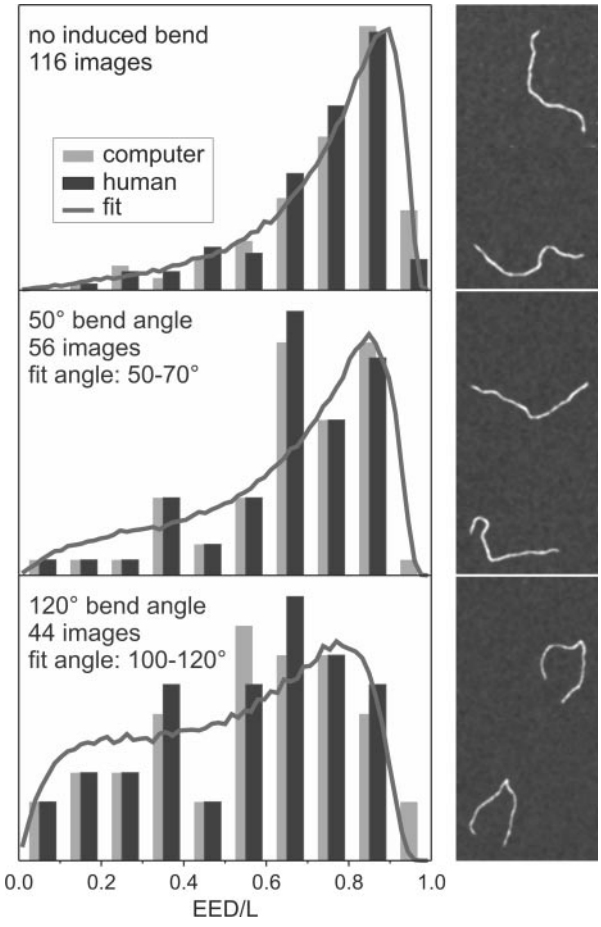

Figure 3. Consistency of manual tracing of molecules and simulation-based analysis. Simulated molecules were digitized onto a grid and convolved with a Gaussian kernel resulting in the images on the right. Their contour lengths *L* and EEDs are manually traced and shown as 'human' in the histograms. The numbers extracted directly from the simulations yield the histograms indicated with 'computer'. No significant deviations are observed, validating the manual tracing approach. Next, we subjected these data to the fitting procedure described in the text. From the 0° data set, we obtain a persistence length of *L*/4, exactly as imposed in the simulation. The data sets with 50° and 120° induced bending angles yield the angle ranges indicated in their respective histograms, confirming the validity of the procedure.

The EED distributions obtained from our experiments were fitted to simulated histograms using a least-squares minimization procedure. Using this method, a value for the induced bending angle and its statistical uncertainty is obtained, as described in Materials and Methods. The fitting procedure is performed easily using only EED and *L* data, which are in turn extracted from SFM images in a straightforward manner.

To validate this approach, we generated images from ~200 simulated molecules with 0°, 50° and 120° angles, which strongly resembled the experimentally obtained images after a Gaussian convolution (to mimic tip convolution effects). We then subjected these images to the same analytical procedure, while keeping the simulation parameters hidden to the operator to eliminate biased analysis. The results are shown in Figure 3. From the histograms and the corresponding fit results, it can be concluded that the procedure successfully reproduces the input parameters.

Estimation of the DNA bending angle

The bending angles extracted from our SFM-imaged protein–DNA complexes using the method described above are shown in Table 1. In most cases, the measured EED distributions of the bare DNA and the protein–DNA complexes could be well fit to the distributions obtained from our simulations, yielding reliable estimates of the bend angle (Figure 4a–c, e–j). One data set (NFI–DNA complexes) appeared to be shifted to anomalously low EEDs (Figure 4d). As a consequence, it could not be well fit to any simulated histogram and a bending angle could, therefore, not be determined unambiguously. A possible explanation is that the NFI–DNA complexes had not fully equilibrated in 2D, but rather had a configuration resembling that of DNA molecules trapped from solution (35). Alternatively, a systematic overestimation of the contour length would explain the shifted appearance of this histogram. Indeed, the average value for the contour length for this particular data set was ~20 nm longer than expected from the number of base pairs.

Table 1. DNA bending angles for the protein–DNA complexes of interest obtained using different methods

	Simulations	msEED method (17,24)	Tangent method	Gel retardation/ DNA cyclization	X-ray
NFI	N.D.	46	60 ± 19° (29)	–	–
NFI–4 G/C	20 ± 20°	20	33 ± 14° (29)	–	–
NFI–6 G/C	20 ± 20°	N.D.[a]	37 ± 17° (29)	–	–
Oct-1	40 ± 20°	41	42 ± 12° (30)	37° (34)	–
Oct-1-4 G/C	40 ± 20°	29	39 ± 15° (40)	–	–
XPC-HR23B	50 ± 10°	54	39 ± 24° (28)	–	–
IHF	110 ± 20°	N.D.	64 ± 20° (this work)/ 50 ± 27 (20)/123° (19)	140° (6)/120–180° (7)	160° (10)

[a]No value could be calculated for this data set using the msEED method, which in this case implies a bending angle close to zero.

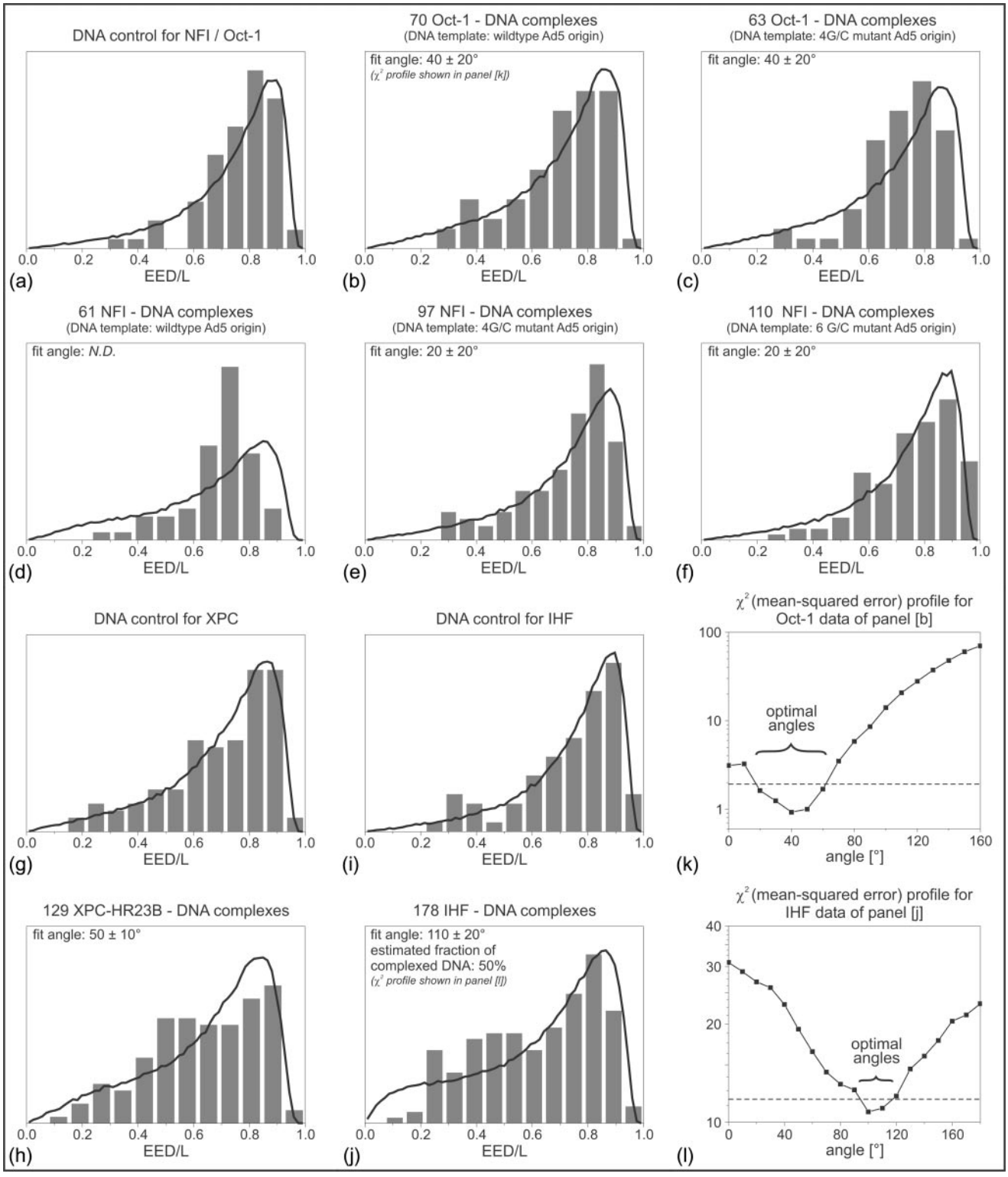

Figure 4. (**a**–**j**) Histograms of experimentally obtained values for EED normalized by contour lengths *L* of bare DNA molecules and protein–DNA complexes and the corresponding fits. (**k**–**l**) χ^2 profiles for the data sets (solid lines with squares). The intersections with the dashed line indicate the uncertainty in the angle determination (33).

In the case of IHF (Figure 4j), the protein often cannot be distinguished in the SFM images. We have, therefore, fitted the IHF–EED data to simulated bent-DNA histograms augmented in an adjustable ratio with an unbent-DNA histogram, to accommodate for a fraction of DNA molecules with no IHF bound. The best fit was obtained assuming that ~50% of the DNA molecules had IHF bound. As a control, we applied a tangent method to the images. The bimodal distribution of

bending angles that we found (Figure 1c) elegantly confirms that ~50% of the DNA molecules has IHF bound and has been bent (64 ± 20°).

In order to relate to the values estimated using our simulations, Table 1 also displays values of bending angles obtained using the mean squared end-to-end distance (msEED) method [introduced by Rivetti *et al*. (17)], the tangent method and biochemical methods. The bending angles obtained using the simulations are in good agreement with values obtained using the msEED method and biochemical techniques. Using biochemical techniques and X-ray crystallography, the bending angle induced by IHF had been estimated between 120° and 180° (6,7,10,14,37). Similarly, using gel retardation and circularization experiments a bending angle of 37° had been determined for Oct-1 (38). Note that the msEED approach cannot be applied to the mixed population of bent/unbent molecules in the case of IHF. The agreement between the various methods provides another validation for our approach. However, there are clear differences among SFM-based measurements of the IHF- and XPC-HR23B-induced bending angle. The bending angles for these relatively strongly bending proteins are underestimated using the tangent method instead of the two EED-based analysis methods. An apparent exception to this tendency is the IHF bending angle reported by Seong *et al*. (19). However, this is probably due to their deposition procedure, which projects the DNA molecules in its 3D conformation onto the surface. This procedure probably exaggerates the induced angle, thus effectively compensating for the underestimation of large bend angles that seems to be associated with the tangent method.

Comparison of the IHF results suggests that the tangent method leads to underestimation when the DNA is strongly bent. This is probably due to the limited resolution and the consequent difficulty of accurately choosing a proper tangent vector at the site of the bend. Our method is based on the estimation of a bending angle from intrinsic properties of the polymer. This type of estimate is neither affected by operator bias nor by tip convolution effects resulting in difficulties determining the tangents. In principle, the method can, therefore, be equally well applied to DNA with low and high degrees of protein-induced bending. However, in the case of low bend angles the end-to-end distributions change only marginally with respect to those of unbent DNA. Therefore, accurate determination of low degrees of bending requires a distribution with reduced statistical noise (implying the need for more data), such that the data can be more unequivocally fit. We wish to emphasize that, although the relatively large reported uncertainty of bending angles might suggest the simulation-based analysis to be less accurate, error margins reported in studies based on a tangent method often do not take systematic errors like those listed above into account.

A number of marked advantages of our present method become apparent when compared with other methods. First, our method shares with the msEED method improved reliability of bend angle estimates due to their robustness and immunity for SFM tip convolution effects, to which the tangent method is sensitive. Moreover, they significantly reduce the time required for the actual analysis, which potentially allows for much better statistics. Second, using our distribution-based method, irregular distributions as seen for NFI on the wild-type Ad5 origin (Figure 4d) can be immediately disregarded, whereas the msEED and tangent methods yield a potentially unreliable value (Table 1). If the data cannot be fit with the simulations like in the case of NFI–DNA (Figure 4d), the DNA may have been ill equilibrated in 2D on the surface. Improper equilibration strongly decreases the reliability of bending angle analysis using the tangent method. Equilibration is key to reliable application of the msEED and simulation-based approaches. Hence, besides being a tool to analyze DNA bending angles, our method can also be used to assess the 'quality' of the deposition of the DNA on mica. Third, the present method does not require a visible feature at the site of bending, as exemplified by the case of IHF–DNA complexes. This property also extends the applicability to the analysis of DNA deformations, such as those induced by particular sequences or chemical adducts. Another advantage of the simulation-based approach is that it can in principle be adapted for more complex situations. For example, one could consider (protein-induced) bends that are variable rather than fixed (hinges) or multiple bends per molecule, whether or not at a defined site. These situations are virtually inaccessible to analytical approaches like the msEED method, yet readily implemented in our simulations.

ACKNOWLEDGEMENTS

Nora Goosen (Leiden University) is kindly acknowledged for the donation of IHF and the vector pGP160. We also thank Fred MacKintosh (Vrije Universiteit) for his useful suggestions regarding the simulations. We benefited from discussions with Bram van den Broek and Wim Sterrenburg (Vrije Universiteit) concerning the statistics of our fitting procedure. This work was financially supported by an ALW-NWO Open competition grant (R.T.D. and G.J.L.W.), a grant within the FOM Biomolecular Physics program (J.v.M. and G.J.L.W.) and NWO Vernieuwingsimpuls (G.J.L.W.). The software written for our simulation-based analysis of bending angles is available for download from our website at http://www.nat.vu.nl/compl/bendinganalysis free of charge. Funding to pay the Open Access publication charges for this article was provided by the Vrije Universiteit, Amsterdam.

Conflict of interest statement. None declared.

REFERENCES

1. Harrington,R.E. (1992) DNA curving and bending in protein–DNA recognition. *Mol. Microbiol.*, **6**, 2549–2555.
2. van der Vliet,P.C. and Verrijzer,C.P. (1993) Bending of DNA by transcription factors. *Bioessays*, **15**, 25–32.
3. Van Noort,J., Verbrugge,S., Goosen,N., Dekker,C. and Dame,R.T. (2004) Dual architectural roles of HU: formation of flexible hinges and rigid filaments. *Proc. Natl Acad. Sci. USA*, **101**, 6969–6974.
4. Ali,B.M., Amit,R., Braslavsky,I., Oppenheim,A.B., Gileadi,O. and Stavans,J. (2001) Compaction of single DNA molecules induced by binding of integration host factor (IHF). *Proc. Natl Acad. Sci. USA*, **98**, 10658–10663.
5. Dame,R.T. (2005) The role of nucleoid-associated proteins in the organization and compaction of bacterial chromatin. *Mol. Microbiol.*, doi:10.1111/j.1365-2958.2005.04598.x.

6. Thompson,J.F. and Landy,A. (1988) Empirical estimation of protein-induced DNA bending angles: applications to lambda site-specific recombination complexes. *Nucleic Acids Res.*, **16**, 9687–9705.
7. Sun,D., Hurley,L.H. and Harshey,R.M. (1996) Structural distortions induced by integration host factor (IHF) at the H′ site of phage lambda probed by (+)-CC-1065, pluramycin, and $KMnO_4$ and by DNA cyclization studies. *Biochemistry*, **35**, 10815–10827.
8. Swinger,K.K., Lemberg,K.M., Zhang,Y. and Rice,P.A. (2003) Flexible DNA bending in HU–DNA cocrystal structures. *EMBO J.*, **22**, 3749–3760.
9. Murphy,F.V., Sweet,R.M. and Churchill,M.E. (1999) The structure of a chromosomal high mobility group protein–DNA complex reveals sequence-neutral mechanisms important for non-sequence-specific DNA recognition. *EMBO J.*, **18**, 6610–6618.
10. Rice,P.A., Yang,S., Mizuuchi,K. and Nash,H.A. (1996) Crystal structure of an IHF–DNA complex: a protein-induced DNA U-turn. *Cell*, **87**, 1295–1306.
11. Jamieson,E.R., Jacobson,M.P., Barnes,C.M., Chow,C.S. and Lippard,S.J. (1999) Structural and kinetic studies of a cisplatin-modified DNA icosamer binding to HMG1 domain B. *J. Biol. Chem.*, **274**, 12346–12354.
12. Wojtuszewski,K. and Mukerji,I. (2003) HU binding to bent DNA: a fluorescence resonance energy transfer and anisotropy study. *Biochemistry*, **42**, 3096–3104.
13. Lorenz,M., Hillisch,A., Payet,D., Buttinelli,M., Travers,A. and Diekmann,S. (1999) DNA bending induced by high mobility group proteins studied by fluorescence resonance energy transfer. *Biochemistry*, **38**, 12150–12158.
14. Lorenz,M., Hillisch,A., Goodman,S.D. and Diekmann,S. (1999) Global structure similarities of intact and nicked DNA complexed with IHF measured in solution by fluorescence resonance energy transfer. *Nucleic Acids Res.*, **27**, 4619–4625.
15. Dame,R.T., Wyman,C. and Goosen,N. (2003) Insights into the regulation of transcription by scanning force microscopy. *J. Microsc.*, **212**, 244–253.
16. Bustamante,C. and Rivetti,C. (1996) Visualizing protein–nucleic acid interactions on a large scale with the scanning force microscope. *Annu. Rev. Biophys. Biomol. Struct.*, **25**, 395–429.
17. Rivetti,C., Walker,C. and Bustamante,C. (1998) Polymer chain statistics and conformational analysis of DNA molecules with bends or sections of different flexibility. *J. Mol. Biol.*, **280**, 41–59.
18. Erie,D.A., Yang,G., Schultz,H.C. and Bustamante,C. (1994) DNA bending by Cro protein in specific and nonspecific complexes: implications for protein site recognition and specificity. *Science*, **266**, 1562–1566.
19. Seong,G.H., Kobatake,E., Miura,K., Nakazawa,A. and Aizawa,M. (2002) Direct atomic force microscopy visualization of integration host factor-induced DNA bending structure of the promoter regulatory region on the Pseudomonas TOL plasmid. *Biochem. Biophys. Res. Commun.*, **291**, 361–366.
20. Sieira,R., Comerci,D.J., Pietrasanta,L.I. and Ugalde,R.A. (2004) Integration host factor is involved in transcriptional regulation of the *Brucella abortus* virB operon. *Mol. Microbiol.*, **54**, 808–822.
21. Kratky,O. and Porod,G. (1949) Röntgenuntersuchung aufgelöster Fademolekule. *Recueil*, **68**, 1106–1122.
22. Schellman,J.A. (1974) Flexibility of DNA. *Biopolymers*, **13**, 217–226.
23. Lu,Y., Weers,B.D. and Stellwagen,N.C. (2003) Analysis of the intrinsic bend in the M13 origin of replication by atomic force microscopy. *Biophys. J.*, **85**, 409–415.
24. Rivetti,C., Guthold,M. and Bustamante,C. (1999) Wrapping of DNA around the *E.coli* RNA polymerase open promoter complex. *EMBO J.*, **18**, 4464–4475.
25. Wilhelm,J. and Frey,E. (1996) Radial distribution function of semiflexible polymers. *Phys. Rev. Lett.*, **77**, 2581–2584.
26. Goosen,N. (1984) Regulation of transposition of bacteriophage Mu. PhD Thesis, State University of Leiden, Leiden, The Netherlands.
27. Dame,R.T., Wyman,C. and Goosen,N. (2001) Structural basis for preferential binding of H-NS to curved DNA. *Biochimie*, **83**, 231–234.
28. Janicijevic,A., Sugasawa,K., Shimizu,Y., Hanaoka,F., Wijgers,N., Djurica,M., Hoeijmakers,J.H. and Wyman,C. (2003) DNA bending by the human damage recognition complex XPC-HR23B. *DNA Repair (Amst.)*, **2**, 325–336.
29. Mysiak,M.E., Bleijenberg,M.H., Wyman,C., Holthuizen,P.E. and van der Vliet,P.C. (2004) Bending of adenovirus origin DNA by nuclear factor I as shown by scanning force microscopy is required for optimal DNA replication. *J. Virol.*, **78**, 1928–1935.
30. Mysiak,M.E., Wyman,C., Holthuizen,P.E. and van der Vliet,P.C. (2004) NFI anc Oct-1 bend the Ad5 origin in the same direction leading to optimal DNA replication. *Nucleic Acids Res.*, **32**, 6218–6225.
31. Watson,J.D. and Crick,F.H.C. (1953) Molecular structure of nucleic acids: a structure for deoxyribose nucleic acid. *Nature*, **171**, 737–738.
32. Almeida,F.M.L., Barbi,M. and do Vale,M.A.B. (2000) A proposal for a different chi-square function for Poisson distributions. *Nucl. Instrum. Meth. A*, **449**, 383–395.
33. Bevington,P.R. and Robinson,D.K. (2003) *Data Reduction and Error Analysis for the Physical Sciences, 3rd edn*. McGraw-Hill, Boston, MA.
34. Verrijzer,C.P., van Oosterhout,J.A., van Weperen,W.W. and van der Vliet,P.C. (1991) POU proteins bend DNA via the POU-specific domain. *EMBO J.*, **10**, 3007–3014.
35. Rivetti,C., Guthold,M. and Bustamante,C. (1996) Scanning force microscopy of DNA deposited onto mica: equilibration versus kinetic trapping studied by statistical polymer chain analysis. *J. Mol. Biol.*, **264**, 919–932.
36. Rivetti,C. and Codeluppi,S. (2001) Accurate length determination of DNA molecules visualized by atomic force microscopy: evidence for a partial B- to A-form transition on mica. *Ultramicroscopy*, **87**, 55–66.
37. Dame,R.T. (2003) Architectural roles of H-NS and HU in DNA compaction and transcription regulation. PhD Thesis, Leiden University, Leiden, The Netherlands.
38. Thompson,J.F. and Landy,A. (1991) POU proteins bend DNA via the POU-specific domain. *EMBO J.*, **10**, 3007–3014.
39. Sun,D., Kobatake,E. and Harshey,R.M. (2002) Structural distortions induced by integration host factor (IHF) at the promoter regulatory region on the Pseudomonas TOL plasmid. *Biochemistry*, **35**, 361–366.
40. Mysiak,M.E. (2004) Molecular architecture of the preinitiation complex in adenovirus DNA replication. PhD Thesis, Utrecht University, Utrecht, The Netherlands.